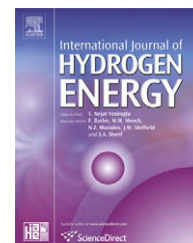


Available at [www.sciencedirect.com](http://www.sciencedirect.com)journal homepage: [www.elsevier.com/locate/he](http://www.elsevier.com/locate/he)

# Role of mixture richness, spark and valve timing in hydrogen-fuelled engine performance and emission

Farhad Salimi\*, Amir H. Shamekhi, Ali M. Pourkhesalian

Mechanical Engineering Dept., K.N.Toosi University of Technology, No. 15, Pardis St., MolaSadra Ave., Vanak Sq., Tehran, Iran

## ARTICLE INFO

### Article history:

Received 11 November 2008

Received in revised form

1 February 2009

Accepted 2 February 2009

Available online 5 April 2009

### Keywords:

Air to fuel ratio

Spark advance

Valve timing

Emission

Performance

## ABSTRACT

The use of hydrogen as an engine fuel has a great potential for reducing exhaust emissions. With the exception of a little amount of hydrocarbon emissions originating from the lubricating oil,  $\text{NO}_x$  is the only pollutant emitted. The special properties of hydrogen compel much more study on hydrogen internal combustion engines (ICEs). Studying and analyzing the behavior of hydrogen ICE and its sensitivity to controllable parameters can help designers to have better understanding over hydrogen characteristics and its combustion in an ICE. In this paper, firstly a quasi-dimensional two-zone thermodynamic model of an SI hydrogen ICE is developed and validated by experimental data. The model is used as an engine simulator. Spark advance (SA), air to fuel ratio and valve timing are selected as the main effective and controllable parameters on engine emissions and performance characteristics. Valve timing parameter is defined as the intake and exhaust valves' lift, opening time and duration. Secondly, the effects of variation of the mentioned three parameters on emission and performance characteristics of the modeled engine are illustrated. Finally, the reasons of the engine behavior and characteristics under variations of these parameters are fully discussed.

© 2009 International Association for Hydrogen Energy. Published by Elsevier Ltd. All rights reserved.

## 1. Introduction

Hydrogen can be produced from many different sources, such as natural gas, coal, biomass and water. The potential role of hydrogen in global warming, which nowadays is a hot topic, is insignificant in comparison to hydrocarbon-based fuels. The reason is that combustion of hydrogen produces no carbon-based compounds such as HC, CO, and  $\text{CO}_2$ .

Hydrogen has special properties so the combustion characteristics of hydrogen are very different from gasoline. The laminar flame speed of a hydrogen air mixture at stoichiometric condition is about 10 times that of gasoline. The wide flammability limit of hydrogen allows the use of very low

equivalence ratios which result in reducing  $\text{NO}_x$  emissions. The octane rating of hydrogen of 106 RON allows increasing compression ratio.

Hydrogen is one of the most interesting alternative fuels, and is recently in the centre of attention. Hydrogen is renewable and offers lots of other benefits. The most practical one is its ability to run in bi-fuel conditions.

Hydrogen internal combustion engines have the ability for increasing efficiency [1]. Comprehensive overview of hydrogen engine properties and design features is already done by previous authors and it was concluded that hydrogen internal combustion engines have a high efficiency, are very clean and considerably cheaper than fuel cells [2].

\* Corresponding author. Tel.: +98 21840563246; fax: +98 2188674747.

E-mail addresses: [salimi84@yahoo.com](mailto:salimi84@yahoo.com) (F. Salimi), [shamekhi@kntu.ac.ir](mailto:shamekhi@kntu.ac.ir) (A.H. Shamekhi), [pourkhesalian@yahoo.com](mailto:pourkhesalian@yahoo.com) (A.M. Pourkhesalian).

0360-3199/\$ – see front matter © 2009 International Association for Hydrogen Energy. Published by Elsevier Ltd. All rights reserved.  
doi:10.1016/j.ijhydene.2009.02.077

Nomenclature:	
<i>Symbols</i>	
A/F	air to fuel
$A_R$	reference area
atm	atmosphere
$c_D$	discharge coefficient
$c_v$	specific heat at constant volume
$c_p$	specific heat at constant pressure
$D_V$	valve diameter
$e$	specific energy
$E$	energy
$H$	special enthalpy
hp	horse power
$L_V$	valve lift
$m$	mass
$m_l$	leakage mass (due to blowby)
$\dot{m}$	mass flow rate
$NO_x$	nitric oxides
$P$	pressure
$P_o$	stagnation pressure
$P_b$	brake power
$P_T$	pressure at the restriction
$Q$	heat transfer
$R$	gas constant
$T$	temperature
$V$	volume
$u$	burning velocity
$u'$	root mean square turbulent velocity
$W$	work transfer
$\bar{U}_p$	mean piston speed
$\alpha_T$	temperature exponent
$\beta_P$	pressure exponent
$\phi$	fuel to air equivalence ratio
$\theta$	crank angle
$\gamma$	specific heat ratio
$\rho$	density
<i>Acronyms</i>	
BTDC	before top dead centre
CA	crank angle
CI	compression ignition
EVO	exhaust valve opening
IVO	intake valve opening
RON	research octane number
SA	spark advance
TDC	top dead centre
VVT	variable valve timing
SI	spark ignition
rpm	revolution per minute
ppm	particles per million
BMEP	break mean effective pressure
ICE	internal combustion engine
<i>Subscripts</i>	
0	reference condition
$b$	burned
$f$	flame
$l$	laminar
$t$	turbulent
$u$	unburned

Limited numbers of previous publications have worked on hydrogen-fuelled engine simulation. A two-zone quasi-dimensional engine model for calculating power and  $NO_x$  emission was demonstrated by Fagelson et al. [3]. In their work, laminar burning velocity is calculated from a second order reaction with estimated activation energy.

Kumar et al. [4] used the same model in order to predict the performance of a supercharged hydrogen engine. They report an overestimation of the rate of pressure rise that can be a consequence of an overestimation in burning velocity. Ma et al. [5] used Wiebe's law in a zero-dimensional model. And for a varying compression ratio and ignition timing the optimum cylinder diameter for a fixed equivalence ratio was calculated.

Verhelst et al. [6] preferred quasi-dimensional model to multi-dimensional one because of a reasonable accuracy and fast computation on PC system. They developed a complete cycle simulation code for SI engine and they looked thoroughly at the turbulent combustion in a hydrogen-fuelled engine. In another reference [7] a simulation and design tool applicable to hydrogen powered spark ignition engine systems is introduced. The model is applicable to single and multi-cylinder engines under steady state or transient operating conditions. The model is validated against experimental data for the intake flow model. In a recent publication [8] a 3D CFD modeling of combustion and nitrogen oxide formation in

hydrogen-fuelled ICEs has been developed and it was concluded that the mixture heterogeneity is a key parameter to control the combustion spreading and  $NO_x$  formation during combustion.

In this paper, first of all a quasi-dimensional code for the four strokes of SI hydrogen engine is developed. In the model the turbulent flame speed is modeled based on previous literature. The model then is calibrated by matching the data obtained in the previous experiment [9]. Spark advance (SA), air to fuel ratio, valve timing is chosen as the most effective parameters on hydrogen-fuelled engine behavior. Valve timing is defined as the intake and exhaust valves' lift, opening time and duration. Effects of variations of these parameters on engine emissions and performance characteristics are also illustrated. The mentioned trends then were fully studied and discussed.

## 2. Engine model

The engine model is a quasi-dimensional two-zone model which solves the basic differential equations for intake, compression, power and exhaust strokes.

In this model, the combustion chamber is divided into two zones, which one should imagine as being divided by flame

front, zone 1 contains unburned mixture and zone 2 contains burned mixture. Thermal  $\text{NO}_x$  formation also takes place in burned zone, which is described by the extended Zeldovich mechanism [10]. The flame front is assumed to travel by a speed called turbulent flame speed. Turbulent flame speed is a function of laminar flame speed. Laminar flame speed is computed from previous studies [11]. The engine model uses Woschni correlation [12] to estimate engine heat transfer and burned and unburned zones are calculated by assuming that the flame travels in a semi sphere-like shape. The engine model also includes a friction model to predict brake mean effective pressure. The frictional processes in an internal combustion engine can be categorized into three main components: (1) the mechanical friction, (2) the pumping work, and (3) the accessory work. A method, in which the total friction work is calculated, was used in this work [13]. The applied friction model spontaneously predicts all the above mentioned categories.

The composition of the reaction products is calculated from the chemical equilibrium at a given pressure and temperature of the 12 species  $\text{N}_2$ ,  $\text{NO}$ ,  $\text{N}$ ,  $\text{CO}_2$ ,  $\text{CO}$ ,  $\text{OH}$ ,  $\text{H}$ ,  $\text{O}_2$ ,  $\text{O}$ ,  $\text{H}_2\text{O}$ ,  $\text{H}_2$  and  $\text{Ar}$ . An optimization calculation procedure is used to calculate the mole fraction of each species and the total mole fraction [14].

The engine model is validated by comparing the simulated results with the experimental data taken from a previous engine experiment [9]. The engine used in the experimental evaluation is a dedicated hydrogen-fuelled engine. The dedicated hydrogen-fuelled engine is the descendant of a gasoline-fuelled engine, which was later converted to hydrogen-fuelled one.

## 2.1. Quasi-dimensional model formulations

The basic equation for the engine model which can be derived from the 1st law of thermodynamics is:

$$dE = -\delta Q - \delta W + \sum_i h_i dm_i \quad (1)$$

where,  $E$  is the internal energy of the cylinder gas mixture,  $Q$  is the heat exchange of the cylinder contents with the cylinder walls where  $Q > 0$  for heat loss from gas to wall,  $W$  is the work where  $W > 0$  for work delivered by the cylinder charge,  $h_i$  is the specific enthalpy of gas which enters or leaves the cylinder, and  $dm_i$  is the mass flow into (+) or out of (-) the cylinder. The work  $\delta W$  can be expressed as  $PdV$ , where  $P$  is the pressure and  $V$  is the cylinder volume.

### 2.1.1. Intake and exhaust

The mass flow rate through a valve is usually described by the equation for compressible flow through a flow restriction. This equation is derived from a one-dimensional isentropic flow analysis, and real gas flow effects are included by means of an experimentally determined discharge coefficient  $C_v$ . The air flow rate is related to the upstream stagnation pressure  $P_o$  and stagnation temperature  $T_o$ , static pressure just downstream of the flow restriction (assumed equal to the pressure at the restriction,  $P_t$ ), and a reference area  $A_R$  characteristic of the valve design:

$$\dot{m} = \frac{C_D A_R P_o}{(RT_o)^{1/2}} \left(\frac{P}{P_o}\right)^{1/\gamma} \left\{ \frac{2\gamma}{\gamma-1} \left[ 1 - \left(\frac{P_T}{P_o}\right)^{(\gamma-1)/\gamma} \right] \right\}^{1/2} \quad (2)$$

When the flow is choked, i.e.,  $(P_T/P_o) \leq [2/(\gamma+1)]^{\gamma/(\gamma-1)}$  the appropriate equation is:

$$\dot{m} = \frac{C_D A_R P_o}{(RT_o)^{1/2}} \gamma^{1/2} \left(\frac{2}{\gamma+1}\right)^{(\gamma+1)/2(\gamma-1)} \quad (3)$$

For flow into the cylinder through an intake valve,  $P_o$  is the intake system pressure and  $P_T$  is the cylinder pressure. For flow out of the cylinder through an exhaust valve,  $P_o$  is the cylinder pressure and  $P_T$  is the exhaust system pressure. Several different reference areas can be used. In this paper, the so-called valve curtain area was used as reference area:

$$A_R = \pi D_v L_v \quad (4)$$

### 2.1.2. Compression and expansion

During compression and expansion Eq. (1) can be simplified to:

$$\frac{dT}{d\theta} = \frac{1}{mc_v} \left[ -\frac{dQ}{d\theta} - P \frac{dV}{d\theta} + \frac{dm_l}{d\theta} RT \right] \quad (5)$$

where,  $R$  is the mixture gas constant,  $\theta$  is the crank angle and  $dm_l/d\theta$  is the cylinder mass leakage due to blowby. By neglecting the change in gas constant during expansion the rate of pressure change can be calculated from the ideal gas state equation:

$$\frac{dP}{d\theta} = \frac{1}{V} \left[ \frac{dm_l}{d\theta} RT + mR \frac{dT}{d\theta} - P \frac{dV}{d\theta} \right] \quad (6)$$

### 2.1.3. Combustion

Using conservation of mass and energy and the ideal gas equation the rate of change of cylinder pressure  $P$ , unburned and burned gas temperature  $T_u$  and  $T_b$  are:

$$\begin{aligned} \frac{dP}{d\theta} = & \left( \frac{c_{v,u}}{c_{p,u}} - \frac{c_{v,b}}{R_b} \frac{R_u}{c_{p,u}} V_u + \frac{C_{v,b} V}{R_b} \right)^{-1} \left\{ - \left( 1 + \frac{c_{v,b}}{R_b} \right) P \frac{dV}{d\theta} \right. \\ & - C_{p,b} T_b \frac{dm_{l,b}}{d\theta} - \frac{R_u}{R_b} c_{p,b} T_u \frac{dm_{l,u}}{d\theta} - \left[ (e_b - e_u) \right. \\ & \left. \left. - c_{v,b} \left( T_b - \frac{R_u T_u}{R_b} \right) \right] \frac{dm_b}{d\theta} + \left( \frac{c_{v,u}}{c_{p,u}} - \frac{c_{v,b}}{R_b} \frac{R_u}{c_{p,u}} \right) \frac{dQ_u}{d\theta} - \frac{dQ}{d\theta} \right\} \quad (7) \end{aligned}$$

where, subscripts  $u$  and  $b$  denote unburned and burned properties respectively and subscript,  $l$ , denotes leakage (due to blowby).  $c_v$  and  $c_p$  are the specific heats at constant volume and pressure respectively,  $e$  is the specific energy and  $dm_b/d\theta$  is the mass burning rate, which is derived from a turbulent flame speed model.

$$\frac{dT_u}{d\theta} = \frac{1}{m_u c_{p,u}} \left( V_u \frac{dP}{d\theta} - \frac{dQ_u}{d\theta} \right) \quad (8)$$

$$\begin{aligned} \frac{dT_b}{d\theta} = & \frac{P}{m_b R_b} \left[ \frac{dV}{d\theta} - \left( \frac{V_b}{m_b} - \frac{V_u}{m_u} \right) \frac{dm_b}{d\theta} + \frac{V_b}{m_b} \frac{dm_{l,b}}{d\theta} + \frac{V_u}{m_u} \frac{dm_{l,u}}{d\theta} \right. \\ & \left. + \left( \frac{V}{P} - \frac{R_u V_u}{P c_{p,u}} \right) \frac{dP}{d\theta} + \frac{R_u}{P c_{p,u}} \frac{dQ_u}{d\theta} \right] \quad (9) \end{aligned}$$

Then it is assumed that:

$$\frac{dm_b}{d\theta} = \rho_u A_f u_t \quad (10)$$

where  $\rho$  is the density,  $A_f$  is the flame front area and  $u_t$  is the turbulent flame speed.

#### 2.1.4. Laminar flame speed

Flame speed is a critical effective parameter in model results, so using an accurate formulation is essential. Almost all of the turbulent combustion models assume that the combustion happens in flamelet regime. It is then assumed to travel locally at the laminar flame speed therefore it is necessary to know the laminar flame speed of the hydrogen/air mixture. Here, firstly a short overview over hydrogen burning velocity is given.

In Liu and MacFarlane's publication [15] laminar burning velocity of hydrogen/air mixture was measured and their measurements resulted in a formula as a function of fuel/air equivalence ratio and residual gas mole fraction. Milton and Keck [16] took out the laminar burning velocity of stoichiometric hydrogen/air mixture from some experiments. Then, they fitted a correlation to the experimental data. Iljima and Takeno [11] described the laminar burning velocity of hydrogen/air mixture by a zero-dimensional analysis. Other kinds of formulas have been developed by some other authors too, including Koroll et al. [17], Taylor [18], Law et al. [19], Kobayashi et al. [20].

From all the correlations developed by the researchers above only Iljima and Takeno's [11] formula is a function of the three parameters which are fuel/air equivalence ratio, temperature and pressure. The others' formulations do not include one of the above parameters, so their equation has enough integrity that was needed for this work. Therefore, in this paper, Iljima and Takeno's [11] formula is used. In this method flame speed in (m/s) is:

$$u_l = u_{l0} \left( \frac{T_u}{T_o} \right)^{\alpha_T} \left[ 1 + \beta_p \log \frac{P}{P_o} \right] \quad (11)$$

where,  $P$  is the pressure,  $T_u$  is the unburned temperature,  $T_o = 291(K)$ ,  $P_o = 101,325(Pa)$ .

$\alpha_T$  and  $\beta_p$  are as follows:

$$\begin{aligned} \alpha_T &= 1.54 + 0.026(\phi - 1) \\ \beta_p &= 0.43 + 0.003(\phi - 1) \end{aligned} \quad (12)$$

And  $u_{l0}$  which is the laminar burning velocity of hydrogen at 291(K) and 1(atm), in (m/s), is given by:

$$u_{l0} = 2.98 - (\phi - 1)^2 + 0.32(\phi - 1.70)^3 \quad (13)$$

**Table 1 – Engine specifications.**

Displacement volume	430.8 cc
Bore	86.0 mm
Stroke	74.2 mm
Compression ratio	9.7
Intake valve diameter	36.0 mm
Exhaust valve diameter	25.4 mm
Intake valve lift	8.4 mm
Exhaust valve lift	5.7 mm

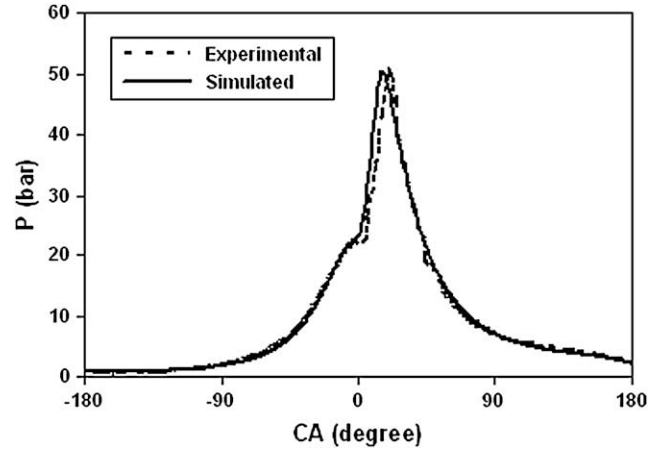


**Fig. 1 – In-cylinder pressure variations versus crank angle at 2830 (rpm),  $\phi = 1.08$ .**

#### 2.1.5. Turbulent flame speed

Many methods for describing and calculating the turbulent flame speed have been developed by previous authors. In this paper, “Damkohler and derivatives” method [21] for turbulent flame speed calculation is used. According to this model turbulent flame speed is as follows:

$$u_t = u' + u_l \quad (14)$$

where:

$$\begin{aligned} u' &= u'_{TDC} \left( 1 - 0.5 \frac{\theta - 360}{45} \right) \\ u'_{TDC} &= 0.75 \bar{U}_p \end{aligned} \quad (15)$$

$\theta$  is the crank angle (360 at TDC of compression) [21,22].

#### 2.1.6. Flame geometry

Eq. (7) needs a flame front area. It is assumed that the flame travels in a semi sphere-like shape centered at spark plug. Also, the spark plug is assumed to be centered. Radius of flame is calculated from flame speed. Considering some geometrical matters the flame front area is calculated.

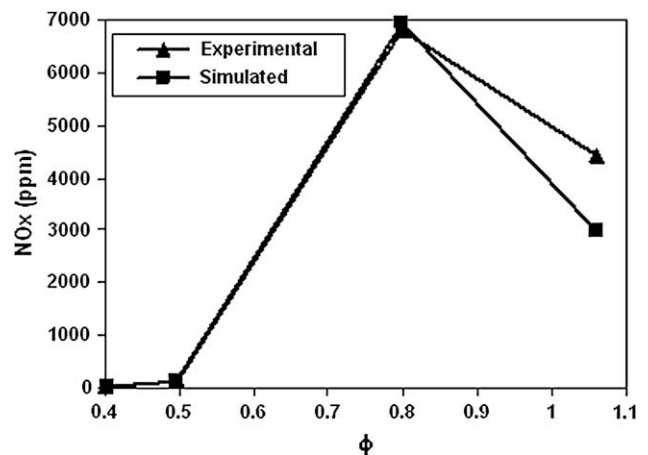


**Fig. 2 – NO<sub>x</sub> concentration variations versus fuel/air equivalence ratio at 2830 (rpm).**

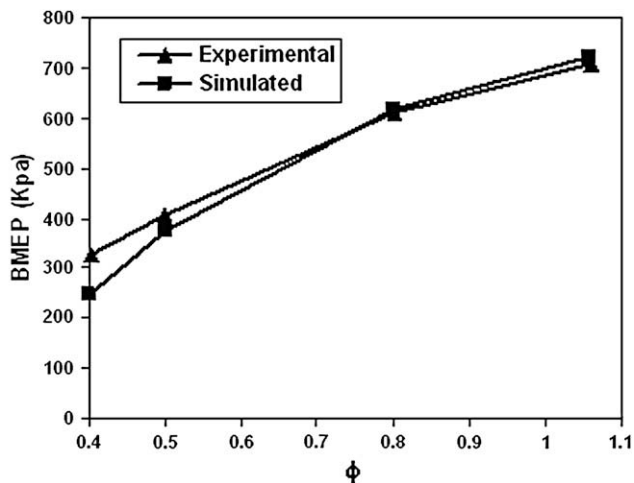


Fig. 3 – BMEP variations versus fuel/air equivalence ratio at 2830 (rpm).

### 3. Model validation

The engine used is a dedicated hydrogen-fuelled engine which was converted from a gasoline engine to bi-fuel operation.

Using the Ijima and Takeno method a two-zone engine model in MATLAB environment is developed. Engine specifications, which can be observed in Table 1, were imported to the model. The simulated data was compared and validated by experimental work [9]. The simulated and experimental in-cylinder pressures versus the crank angle are very close to each other, which can be observed in Fig. 1. This shows that the combination of the mentioned formulations and method work properly.

The results for the experiments and simulated NO<sub>x</sub> concentration versus equivalence fuel/air ratio for some points can be seen in Fig. 2. Also the experimental and simulated results for BMEP versus fuel/air equivalence ratio are shown in Fig. 3. The results are close enough and this shows that the engine model works properly.

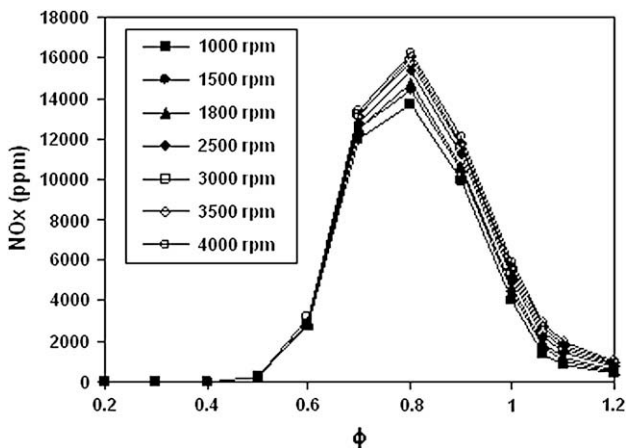


Fig. 4 – NO<sub>x</sub> emission variations versus fuel/air equivalence ratio at different engine speeds.

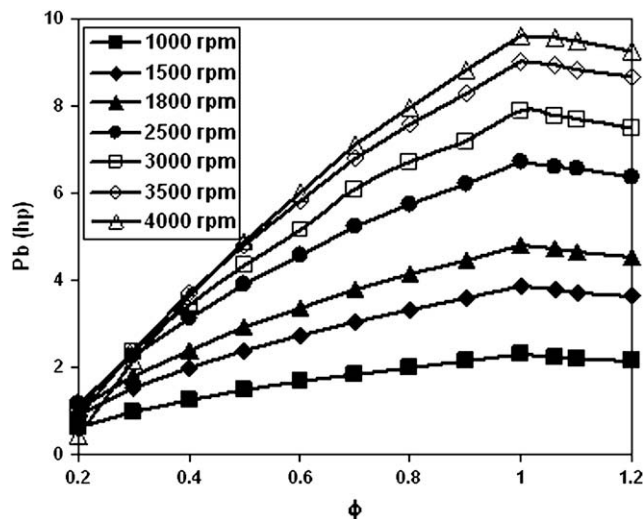


Fig. 5 – Brake power (Pb) variations versus fuel/air equivalence ratio for different engine speeds.

### 4. Air to fuel ratio

A/F ratio plays a very important role in engine performance and emissions characteristics. Hydrogen has special properties and the combustion characteristics of hydrogen are very different from gasoline. The laminar flame speed of a hydrogen air mixture at stoichiometric condition is about 10 times that of gasoline. The wide flammability limit of hydrogen allows the use of very lean fuel/air equivalence ratios, as low as 0.2, which result in reducing NO<sub>x</sub> emissions.

The major effect of A/F ratio on engine NO<sub>x</sub> emission for different engine speeds is shown in Fig. 4. As it is shown the value of NO<sub>x</sub> emission is varied from 16,000 ppm to near zero respecting to fuel/air equivalence ratio. Maximum amount of NO<sub>x</sub> emission occurs when the fuel/air equivalence ratio is about 0.8 and this happens in a wide range of engine speeds.

As it is shown in Fig. 4, NO<sub>x</sub> concentration peaks at near 0.8 fuel/air equivalence ratio, but as the mixture becomes leaner

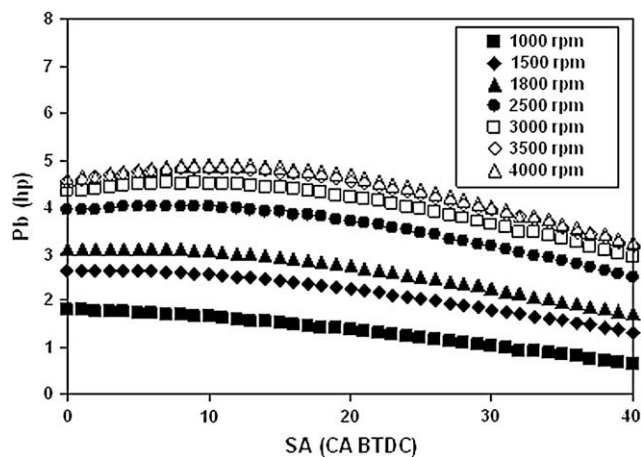


Fig. 6 – Brake power (Pb) variations versus spark advance (SA) for different engine speeds.

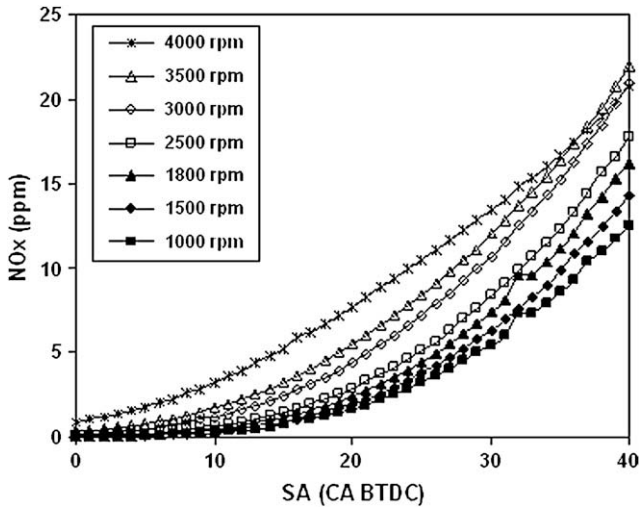


Fig. 7 – NO<sub>x</sub> emission variations versus spark advance (SA) for 2500 (rpm),  $\phi = 0.55$ .

the NO<sub>x</sub> concentration falls dramatically. Maximum burned gas temperature occurs at near 1.1 fuel/air equivalence ratio, but at this equivalence ratio oxygen concentration is low so the NO<sub>x</sub> concentration does not peak there. As the mixture gets richer, burned gas temperature falls. As the mixture gets leaner increasing oxygen concentration initially offsets the falling gas temperature and NO<sub>x</sub> emission peak at near 0.8 fuel/air equivalence ratio.

A/F ratio has a major effect on engine power. This effect is shown in Fig. 5. As it is shown the value of brake power is varied between 1 to near 10 hp respecting to fuel/air equivalence ratio. Maximum amount of brake power occurs when the fuel/air equivalence ratio is about 1, stoichiometric condition, and this happens in a wide range of engine speeds.

As it is seen one of the most important variables in determining SI engine emissions and performance characteristics is the fuel/air equivalence ratio and in hydrogen engines it is much more important. Controlling A/F ratio is really important and effective.

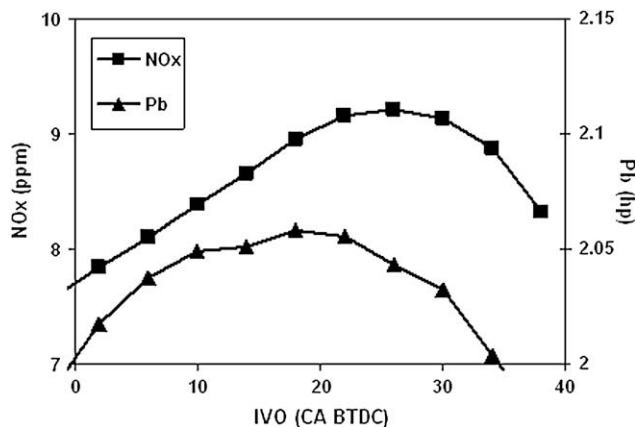


Fig. 8 – NO<sub>x</sub> emission and brake power versus IVO variations for 1500 (rpm),  $\phi = 0.4$ .

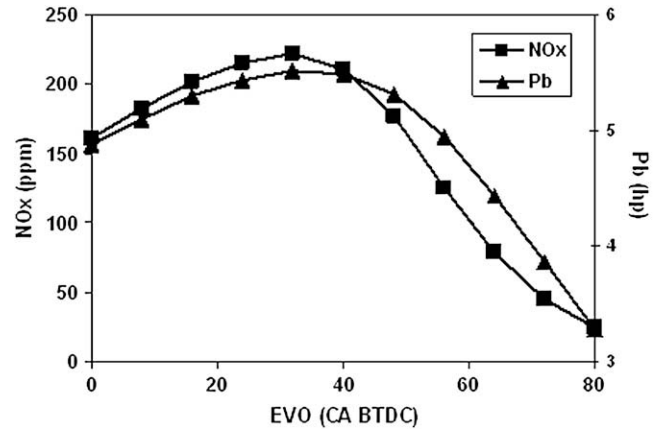


Fig. 9 – NO<sub>x</sub> emission and brake power versus EVO variations for 2500 rpm.

## 5. Spark advance

Spark advance (SA) is another parameter that has a major effect on engine performance and emission. Fig. 6 shows the brake power versus spark advance for different engine speeds. As it is seen in low engine speeds, 1000–1800 (rpm), the maximum power happens when the spark advance range is [5 0] degrees before top dead centre (BTDC). But as the engine speed increases the maximum power happens in more advanced spark, and in 4000 (rpm) this point is near to 10 degrees of crank angle BTDC.

The figure clearly shows that in low engine speeds almost no spark advance is needed, 1–4 degree, and as the engine speed increases, more spark advance is needed. As the spark is advanced the in-cylinder temperature increases and this causes an increase in the NO<sub>x</sub> concentration. This matter is shown in Fig. 7 and it can be seen that the NO<sub>x</sub> varies between about 25 (ppm) and near zero. Since engine knocking is not considered in the model, it should be considered that early spark timing before TDC can lead to engine knocking.

Because of the high hydrogen flame speed, spark advance can be decreased as low as near zero and this is one of the hydrogen-fuelled engine specific properties.

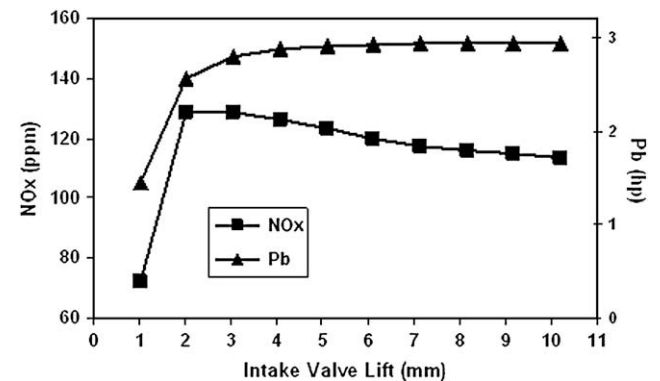


Fig. 10 – NO<sub>x</sub> emission and brake power versus intake valve lift variations for 1000 rpm,  $\phi = 0.5$ .

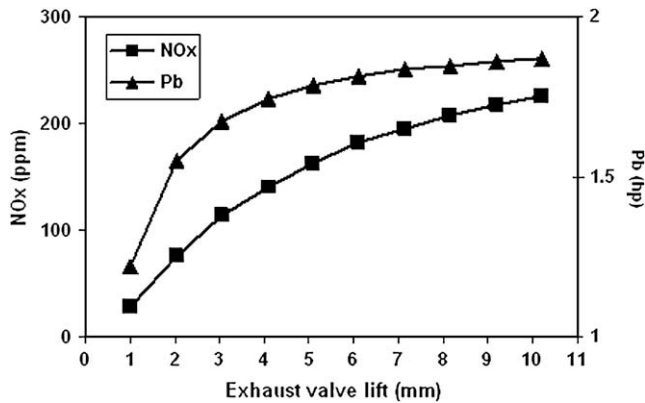


Fig. 11 – NO<sub>x</sub> emission and brake lift power versus exhaust valve lift variations for 1000 (rpm),  $\phi = 0.5$ .

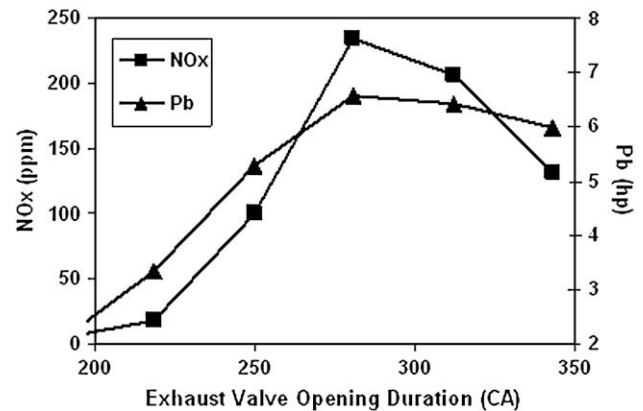


Fig. 13 – NO<sub>x</sub> emission and brake power variations versus exhaust valve opening duration for 3000 (rpm),  $\phi = 0.5$ .

## 6. Valve timing

In internal combustion engines, valves behavior (lift and timing) is one of the most important parameters which has a major effect on the engine operation and emission. By using VVT technology we are able to control engine behavior in any conditions with the purpose of decreasing emission and optimizing engine operating characteristics. The moment of intake and exhaust valves opening has a great effect on engine emission and operation which can be seen on Figs. 8 and 9.

As it is shown in Fig. 8 as the intake valve opening (IVO) advances NO<sub>x</sub> concentration and brake power increase, due to volumetric efficiency increase, and consequently increase of in-cylinder temperature but when the volumetric efficiency approaches its maximum the valves overlap effect shows up. Valves overlap factor increase the amount of residual gas. Any residual burned gas in the unburned mixture reduces the heating value per unit mass of mixture and, thus, reduces the adiabatic flame temperature [10]. Therefore as the residual gas mass fraction increases, brake power decreases and as a result of reduction of in-cylinder temperature, NO<sub>x</sub> concentration falls.

As the EVO advances the exhaust valve opens in higher in-cylinder pressure therefore more burned gas leaves the

cylinder and there is less residual gas so the NO<sub>x</sub> concentration and brake power increase because more fresh mixture enters the cylinder but as the EVO advances more and more, in one point the valves overlap factor overcomes the first effect and therefore residual gas increases and this causes a decrease in NO<sub>x</sub> and brake power. These trends can be seen in Fig. 9.

One of the other effective variables which can be controlled by VVT mechanism is valves (Intake and exhaust) lift. By increasing the intake valve lift the volumetric efficiency and therefore in-cylinder temperature increases and this cause an increase in brake power and NO<sub>x</sub> concentration. Intake valve lift increase also causes an increase in valves overlap factor. So an increase in residual gas and therefore, decrease in NO<sub>x</sub> concentration occurs. These trends can be seen in Fig. 10.

As the exhaust valve lift increases more burned gas leave the cylinder and therefore there is less residual gas in the cylinder and this causes an increase in NO<sub>x</sub> concentration, as it is shown in Fig. 11, as the residual gas decreases more fresh mixture enters the cylinder and brake power increases.

Valves opening duration which is the time between valves (intake or exhaust) opening till closing can be controlled by using VVT mechanism at different conditions.

When the intake valve opening duration increases volumetric efficiency increases too and this causes a rise of in-cylinder temperature and consequently NO<sub>x</sub> concentration grows. As it is shown in Fig. 12 when the duration increases more and more valves overlap factor increases too and therefore residual gas grows and eventually NO<sub>x</sub> concentration reduces.

The mentioned series of events also affects the brake power as well. By increasing the intake valve opening duration brake power increases. But as the duration increases more and more brake power decreases due to an increase in residual gas mass fraction.

As the exhaust valve opening duration increases more burned gas leaves the cylinder so more fresh mixture fills the cylinder in the intake stroke. This causes a sharp increase in brake power and in-cylinder temperature.

Therefore, as it is shown in Fig. 13 NO<sub>x</sub> concentration rises, too. By increasing duration more, the overlap factor increases

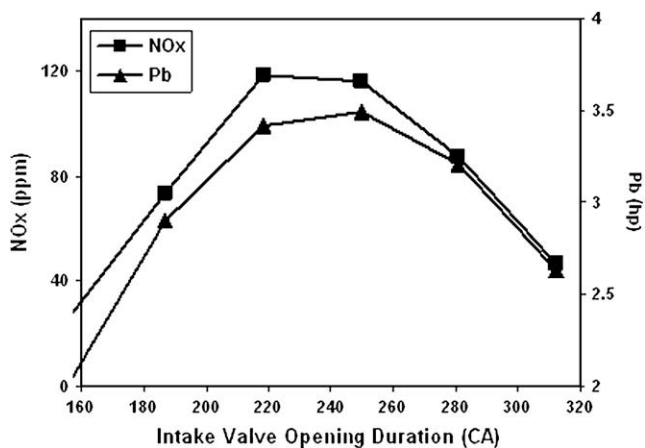


Fig. 12 – NO<sub>x</sub> emission and brake power variations versus intake valve opening duration for 1500 (rpm),  $\phi = 0.5$ .

and consequently residual gas increases, so the  $\text{NO}_x$  concentration and power falls slightly.

## 7. Conclusion

In this work, a quasi-dimensional two-zone thermodynamic model of an SI hydrogen-fuelled engine was developed. The modeled engine results were compared to experimental data. The experimental and simulated results were close enough. So the used formulations and methods in the model were validated. Afterwards, the model was used as an engine simulator to predict engine emission and performance characteristics.

In this paper, also sensitivity of hydrogen engine to variation of spark advance, A/F ratio and valve timing were studied. The importance and effectiveness of the mentioned parameters were illustrated. It was shown that the hydrogen engine has its most  $\text{NO}_x$  concentration at the point near to  $\phi = 0.8$ . Also SA effect was studied and was observed that because of high hydrogen flame speed little advance is needed  $[-5 \ 0]$ . Variation of valves lift, opening time and duration were studied and the reason of their effects fully discussed. The valve timing studies can also be applied to VVT mechanism.

## REFERENCES

- [1] Tang X, Kabat DM, Natkin RJ, Stockhausen WF, Heffel JW. Ford P200 hydrogen engine dynamometer development, SAE paper, 2002-01-0242.
- [2] Verhelst S, Sierens R, Verstraeten S. A critical review of experimental research on hydrogen fueled SI engines. SAE paper, 2006-01-0430.
- [3] Fagelson JJ, McLean WJ, de Boer PCT. Performance and  $\text{NO}_x$  emissions for spark-ignited Combustion engines using alternative fuels – quasi one-dimensional modeling. I. hydrogen fueled engines. *Combustion Science and Technology* 1978;18:47–57.
- [4] Prabhu-Kumar GP, Nagalingam G, Gopalakrishnan KV. Theoretical studies of a spark-Ignited supercharged hydrogen engine. *International Journal of Hydrogen Energy* 1985;10:389–97.
- [5] Ma J, Su Y, Zhou Y, Zhang Z. Simulation and prediction on the performance of a vehicle's hydrogen engine. *International Journal of Hydrogen Energy* 2003;28:77–83.
- [6] Verhelst S, Verstraeten S, Sierens R. Development of a simulation code for hydrogen fuelled SI engines. In: Proceedings ASME Spring Technical Conference, Aachen, May 8–10, 2006 ICES2006-1317.
- [7] Drew Alan N, Timoney David J, Smith William J. A simulation and design tool for hydrogen SI engine systems-validation of the intake hydrogen flow model. *International Journal of Hydrogen Energy* 2007;32:3084–92.
- [8] Knop V, Benkenida A, Jay S, Colin O. Modeling of combustion and nitrogen oxide formation in hydrogen-fuelled internal combustion engines within a 3D CFD code. *International Journal of Hydrogen Energy* 2008;33:5083–9.
- [9] Swain Michael R, Schade Gregory J, Swain Matthew N. Design and testing of a Dedicated Hydrogen-Fueled Engine, SAE paper, 961077.
- [10] Heywood JB. *Internal combustion engine fundamentals*. McGraw-Hill Book Company; 1988.
- [11] Iljima T, Takeno T. Effects of temperature and pressure on burning velocity. *Combustion and Flame* 1986;65: 35–43.
- [12] Woschni G. A universally applicable equation for the instantaneous heat transfer coefficient in the internal combustion engine, SAE paper, 670931.
- [13] Colin Ferguson R, Allan Kirkpatrick T. *Internal combustion engines: applied thermoscience*. 2nd ed. John Wiley & Sons, Inc; 2001.
- [14] Shamekhi AH. Simulation and fuzzy spark advance control in SI engines by ion current sensing, PhD thesis. Department of Mechanical Engineering, K.N. Toosi University of Technology, September 2004.
- [15] Liu DDS, MacFarlane R. Laminar burning velocities of hydrogen–air and hydrogen–air–steam flames. *Combustion and Flame* 1983;49:59–71.
- [16] Milton B, Keck J. Laminar burning velocities in stoichiometric hydrogen and hydrogen–hydrocarbon gas mixtures. *Combustion and Flame* 1984;58:13–22.
- [17] Koroll GW, kumar RK, Bowels EM. Burning velocities of hydrogen–air mixtures. *Combustion and Flame* 1983;94: 330–40.
- [18] Taylor SC. Burning velocity and the influence of flame stretch, PhD thesis. Leeds University; 1991.
- [19] Tse SD, Zhu DL, Law CK. Morphology and burning rates of expanding spherical flames in  $\text{H}_2/\text{O}_2$ /inert mixture up to 60 atmospheres. In: 28th Symp. (Int.) On Combustion; 2000. p. 1793–800.
- [20] Ogami Y, Kobayashi H. A study of laminar burning velocity for  $\text{H}_2/\text{O}_2$ /He premixed hydrogen/air flames at high pressure and high temperature. In: 6th ASME-JSME Thermal Engineering Joint Conference, TED-AJ03-375; 2003.
- [21] Verhelst S. A study of the combustion in hydrogen- fuelled internal combustion engines, PhD thesis. Gent University, Gent, Belgium; 2005.
- [22] Hall MJ, Bracco FV. A study of velocities and turbulence intensities measured in firing and motored engines. SAE paper, 870453.